

Flows of Generalized Oldroyd-B Fluids in Curved Pipes

Marília Pires and Adélia Sequeira

Dedicated to Prof. Herbert Amann on the occasion of his 70th birthday

Abstract. The aim of this work is to present a numerical study of generalized Oldroyd-B flows with shear-thinning viscosity in a curved pipe of circular cross section and arbitrary curvature ratio. Flows are driven by a given pressure gradient and behavior of the solutions is discussed with respect to different rheologic and geometric flow parameters.

Mathematics Subject Classification (2000). Primary 76A05; Secondary 74S05.

Keywords. Curved pipe, finite elements, fluids non-Newtonian.

1. Introduction

Complex rheological phenomena such as shear dependent viscosity, stress relaxation, nonlinear creeping and normal stress differences can be found in many fluids like inks, polymer melts, suspensions, liquids crystals or biological fluids. These properties, which cannot be captured by the classical Navier-Stokes equations, lead to non-constant viscosity or to viscoelastic behavior described by nonlinear relations between the Cauchy stress and the strain tensor. Fluids of this type are called non-Newtonian [20].

There are many ways to generalize the Newtonian law of viscosity. The simplest case is the generalized Newtonian model where the extra-stress incorporates a shear-rate dependent viscosity. However, the generalized Newtonian fluids cannot account for the effects described above, namely the viscoelasticity, but they are often used to model simple flows and to study the flow rate in a pipe, as a function of the pressure drop. Suitable viscoelastic constitutive equations are then

required. In general terms, non-Newtonian viscoelastic fluids exhibit both viscous and elastic properties and can be classified as fluids of differential type, rate type and integral type. We refer to the monographs [5], [15], [26], [29] for relevant issues related to non-Newtonian fluids behavior and modeling. Models of rate type such as Oldroyd-B fluids can predict stress relaxation and are used to describe flows in polymer processing. However they cannot capture the complex rheological behavior of many real fluids, such as blood in which the non-Newtonian viscosity effects are of major importance.

Over the past twenty years, a significant progress has been made in the mathematical analysis of the equations of motion of non-Newtonian viscoelastic fluids. Usually, the constitutive equations lead to highly nonlinear systems of partial differential equations of a combined parabolic-hyperbolic type (or elliptic-hyperbolic, for steady flows) closed with appropriate initial and/or boundary conditions. The study of the behavior of their solutions in different geometries requires the use of specific techniques of nonlinear analysis, such as fixed-point arguments associated to auxiliary linear sub-problems. We refer to [21] and [22] for an introduction to existence results for viscoelastic flows.

The hyperbolic nature of the constitutive equations is responsible for many of the difficulties associated with the numerical simulation of viscoelastic flows. Some factors including singularities in the geometry, boundary layers in the flow and the dominance of the nonlinear terms in the equations, result in numerical instabilities for high values of Weissenberg number (non-dimensional viscoelastic parameter). A variety of alternative numerical methods have been developed to overcome this difficulty, but many challenges still remain, in particular for viscoelastic flows in complex geometries (see, e.g., [16], [17] and the references cited therein).

It is known since the pioneering experimental works of Williams *et al.* [30], Grindley and Gibson [14], and Eustice ([11], [12]) that flows in curved pipes are very challenging and considerably more complex than flows in straight pipes. Due to fluid inertia, a secondary motion appears in addition to the primary axial flow. It is induced by an imbalance between the cross-stream pressure gradient and the centrifugal force and consists of a pair of counter-rotating vortices, which appear even for the most mildly curved pipe. This results in asymmetrical wall stresses with higher shear and low pressure regions ([4], [18], [27]).

Steady fully developed viscous flows in curved pipes of circular, elliptical and annular cross-section of both Newtonian and non-Newtonian fluids, have been studied by several authors ([1]–[4], [13], [19], [23], [24], [27]) following the fundamental work of Dean ([9], [10]) for circular cross-section pipes. Using regular perturbation methods around the curvature ratio, Dean obtained analytical solutions in the case of Newtonian fluids. These results have been extended for a larger range of curvature ratio and Reynolds number, showing the existence of additional pairs of vortices and multiple solutions ([8], [31]).

The great interest in the study of curved pipe flows is due to its wide range of applications in engineering (e.g., hydraulic pipe systems related to corrosion failure) and in biofluid dynamics, such as blood flow in vascular regions of low shear

(in healthy or disease states), where the shear-thinning viscosity and viscoelastic behavior should not be neglected ([6], [7], [25], [28]).

This paper is concerned with the numerical study of the behavior of fully developed flows of shear-thinning generalized Oldroyd-B fluids in curved pipes with circular cross-section and arbitrary curvature ratio, for a prescribed pressure gradient. Numerical results show interesting viscosity and viscoelastic effects: for sufficiently small curvature ratio and certain range of viscosity parameters, the flow field is quite complex, showing counter-clockwise rotation of the secondary streamlines and loss of symmetry of the flow field. Stronger inertial effects result in a deformation of the pair of vortices and rotation of the flow in an opposite direction. These effects become weaker for higher values of the Weissenberg number. We remark that for generalized Oldroyd-B fluids the second normal stress difference is zero, as in the particular case of Oldroyd-B, and consequently the second normal stress difference has no impact on the secondary flows ([13]).

The paper is organized as follows. After introducing the governing equations and formulating the problem in polar toroidal coordinates (Section 2 and 3), we consider in Section 4 the numerical approximation of the steady Oldroyd-B model with non constant shear-dependent viscosity, in the above-described geometry. The original problem is decomposed into a Navier-Stokes system and a tensorial transport equation. Using the finite element method and a fixed point algorithm to couple the auxiliary problems, numerical results are obtained for a certain range of non-dimensional flow parameters (viscosity exponent, Reynolds and Weissenberg numbers) associated to the model. A continuation method is used to find the initial guess of the iterations and to increase the absolute value of the viscosity parameter.

Existence and uniqueness of approximated solutions, as well as a priori error estimates to the coupled full problem have already been proved, under a natural restriction on the curvature ratio (see [2]). In a future work, the systematic numerical study presented in this paper will be complemented by a theoretical analysis to justify the complex qualitative behavior of the combined effects of viscosity, inertial and viscoelastic parameters.

2. Governing equations

This paper is concerned with flows of incompressible viscoelastic Oldroyd-B fluids with shear dependent viscosity in a curved pipe $\Omega \subset \mathbb{R}^3$ with boundary $\partial\Omega$. For these fluids, the extra-stress tensor is related to the kinematic variables through

$$\mathbf{S} + \lambda_1 \overset{\nabla}{\mathbf{S}} = 2 \left(\nu + \nu_0 (1 + |\mathbf{D}\mathbf{u}|^2)^q \right) \mathbf{D}\mathbf{u} + 2\lambda_2 \overset{\nabla}{\mathbf{D}\mathbf{u}}, \quad (2.1)$$

where \mathbf{u} is the velocity field, $\mathbf{D}\mathbf{u} = \frac{1}{2}(\nabla\mathbf{u} + \nabla\mathbf{u}^t) = \frac{1}{2} \left(\frac{\partial u_i}{\partial x_j} + \frac{\partial u_j}{\partial x_i} \right)_{i,j=1,2}$ denotes the symmetric part of the velocity gradient, $|\mathbf{D}\mathbf{u}|$ is the shear rate, q is a real number, ν and ν_0 are nonnegative real numbers satisfying $\nu + \nu_0 > 0$, $\lambda_1 > 0$ and

$\lambda_2 > 0$ are viscoelastic constants. The symbol ∇ denotes the objective derivative of Oldroyd type defined by

$$\overset{\nabla}{\mathbf{S}} = \left(\frac{\partial}{\partial t} + \mathbf{u} \cdot \nabla \right) \mathbf{S} - \mathbf{S} \nabla \mathbf{u} - (\nabla \mathbf{u})^t \mathbf{S}.$$

The Cauchy stress tensor is given by $\mathbf{T} = -p\mathbf{I} + \mathbf{S}$, where p represents the pressure. The equations of conservation of momentum and mass hold in the domain Ω ,

$$\rho \left(\frac{\partial \mathbf{u}}{\partial t} + \mathbf{u} \cdot \nabla \mathbf{u} \right) + \nabla p = \nabla \cdot \mathbf{S} + \mathbf{f}, \quad \nabla \cdot \mathbf{u} = 0, \quad (2.2)$$

where $\rho > 0$ is the (constant) density of the fluid and \mathbf{f} is an external force. We first decompose the extra-stress tensor \mathbf{S} into the sum of its Newtonian part $\boldsymbol{\tau}_s = 2 \frac{\lambda_2}{\lambda_1} D\mathbf{u}$ and its viscoelastic part $\boldsymbol{\tau}$. Introducing the quantities

$$\begin{aligned} x &= \frac{\tilde{x}}{L}, & t &= \frac{U\tilde{t}}{L}, & u &= \frac{\tilde{u}}{U}, & p &= \frac{\tilde{p}L}{(\nu + \nu_0)U}, \\ \boldsymbol{\tau} &= \frac{\tilde{\boldsymbol{\tau}}L}{(\nu + \nu_0)U}, & \mathbf{f} &= \frac{\tilde{\mathbf{f}}L^2}{(\nu + \nu_0)U}, \end{aligned}$$

where the symbol \sim is attached to dimensional parameters (L represents a reference length and U a characteristic velocity of the flow). We also set

$$\varepsilon = 1 - \frac{\lambda_2}{\lambda_1(\nu + \nu_0)}, \quad \eta = \frac{\nu_0}{\nu + \nu_0},$$

and defining the Reynolds number and the Weissenberg number as

$$\mathcal{Re} = \frac{\rho U L}{\nu + \nu_0}, \quad \mathcal{We} = \frac{\lambda_1 U}{L}.$$

we can write (2.1)–(2.2) in dimensionless form

$$\begin{cases} -(1 - \varepsilon) \Delta \mathbf{u} + \mathcal{Re} \left(\frac{\partial \mathbf{u}}{\partial t} + \mathbf{u} \cdot \nabla \mathbf{u} \right) + \nabla p = \mathbf{f} + \nabla \cdot \boldsymbol{\tau}, \\ \nabla \cdot \mathbf{u} = 0, \\ \boldsymbol{\tau} + \mathcal{We} \left(\frac{\partial \boldsymbol{\tau}}{\partial t} + \mathbf{u} \cdot \nabla \boldsymbol{\tau} - g(\nabla \mathbf{u}, \boldsymbol{\tau}) \right) = 2 \left(\varepsilon + \eta \boldsymbol{\sigma}(|D\mathbf{u}|^2) \right) D\mathbf{u}, \end{cases} \quad (2.3)$$

with

$$g(\nabla \mathbf{u}, \boldsymbol{\tau}) = \boldsymbol{\tau} \nabla \mathbf{u} + (\nabla \mathbf{u})^t \boldsymbol{\tau}, \quad \boldsymbol{\sigma}(x) = (1 + x)^q - 1.$$

This system is supplemented with a Dirichlet homogeneous boundary condition

$$\mathbf{u} = \mathbf{0} \text{ on } \partial\Omega.$$

In a simple shear this model predicts shear dependent viscosity (shear-thinning for $q < 0$ and shear-thickening for $q > 0$) and normal stress coefficients Ψ_1 and Ψ_2 given by (see, e.g., [5], [17], [29])

$$\begin{aligned} \Psi_1(|D\mathbf{u}|) &= 2 \left(\varepsilon + \eta \boldsymbol{\sigma}(|D\mathbf{u}|^2) \right) |D\mathbf{u}|^2 \\ \Psi_2(|D\mathbf{u}|) &= 0. \end{aligned}$$

Note that the model reduces to Oldroyd-B when $q = 0$.

3. Equivalent formulation in polar toroidal coordinates

We consider fully developed flows in a curved pipe with circular cross-section (see Figure 1).

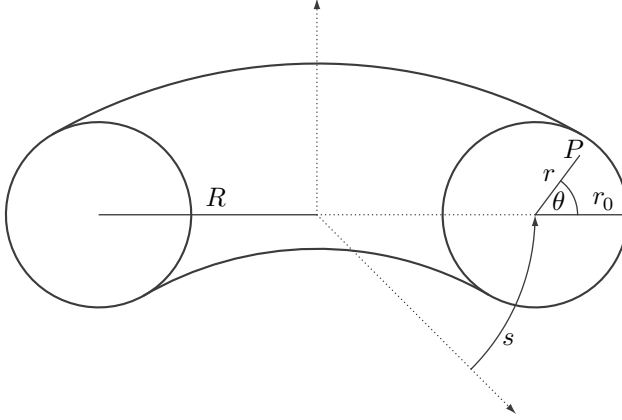


FIGURE 1. Polar toroidal coordinates.

For this pipe geometry, it is more convenient to use the polar toroidal coordinate system, in the variables $(\tilde{r}, \theta, \tilde{s})$, defined with respect to the rectangular cartesian coordinates $(\tilde{x}, \tilde{y}, \tilde{z})$ through the relations

$$\begin{aligned}\tilde{r} &= \sqrt{\tilde{z}^2 + (\sqrt{\tilde{x}^2 + \tilde{y}^2} - R)^2}, \\ \theta &= \arctan \frac{\tilde{z}}{\sqrt{\tilde{x}^2 + \tilde{y}^2} - R}, \quad \tilde{s} = R \arctan \frac{\tilde{y}}{\tilde{x}},\end{aligned}$$

and the inverse relations

$$\tilde{x} = (R + \tilde{r} \cos \theta) \cos \frac{\tilde{s}}{R}, \quad \tilde{y} = (R + \tilde{r} \cos \theta) \sin \frac{\tilde{s}}{R}, \quad \tilde{z} = \tilde{r} \sin \theta,$$

with $0 < r_0 < R$, $0 \leq \theta < 2\pi$ and $0 \leq \tilde{s} < \pi R$, where $R > \tilde{r} \geq 0$ is the constant centerline radius. Introducing

$$s = \frac{\tilde{s}}{r_0}, \quad \delta = \frac{r_0}{R},$$

we see that the corresponding non-dimensional coordinate systems are given by

$$\begin{aligned}r &= \sqrt{z^2 + (\sqrt{x^2 + y^2} - \frac{1}{\delta})^2}, \\ \theta &= \arctan \frac{z}{\sqrt{x^2 + y^2} - \frac{1}{\delta}}, \quad s = \frac{1}{\delta} \arctan \frac{y}{x},\end{aligned}$$

and the inverse relations

$$x = \left(\frac{1}{\delta} + r \cos \theta\right) \cos(s\delta), \quad y = \left(\frac{1}{\delta} + r \cos \theta\right) \sin(s\delta), \quad z = r \sin \theta,$$

with $\delta < 1$, $0 \leq \theta < 2\pi$ and $0 \leq s < \frac{\pi}{\delta}$.

Let us now formulate system (2.3) in this new coordinate system. For convenience, we keep the notation as for the cartesian system (e.g., $u \equiv \mathbf{u} \cdot \mathbf{e}_r$, $v \equiv \mathbf{u} \cdot \mathbf{e}_\theta$ and $w \equiv \mathbf{u} \cdot \mathbf{e}_s$). To simplify the notation we set

$$\begin{aligned}\beta_1 &\equiv \beta_1(r, \theta) = r\delta \sin \theta, & \beta_2 &\equiv \beta_2(r, \theta) = r\delta \cos \theta, \\ \beta &\equiv \beta(r, \theta) = 1 + r\delta \cos \theta.\end{aligned}$$

By using standard arguments, we rewrite the problem (2.3) in the toroidal coordinates (r, θ, s) , and we see that the problem reads as

Find $(\mathbf{u} \equiv (u, v, w), p, \boldsymbol{\tau})$ solution of

$$\left\{ \begin{aligned} & -(\nabla \cdot (2(1-\varepsilon)D\mathbf{u} + \boldsymbol{\tau} - \mathcal{R}e \mathbf{u} \otimes \mathbf{u}))_r + \mathcal{R}e \frac{\partial u}{\partial t} + \frac{\partial p}{\partial r} = 0, \\ & -(\nabla \cdot (2(1-\varepsilon)D\mathbf{u} + \boldsymbol{\tau} - \mathcal{R}e \mathbf{u} \otimes \mathbf{u}))_\theta + \mathcal{R}e \frac{\partial v}{\partial t} + \frac{1}{r} \frac{\partial p}{\partial \theta} = 0, \\ & -(\nabla \cdot (2(1-\varepsilon)D\mathbf{u} + \boldsymbol{\tau} - \mathcal{R}e \mathbf{u} \otimes \mathbf{u}))_s + \mathcal{R}e \frac{\partial w}{\partial t} + \frac{1}{\beta} \frac{\partial p}{\partial s} = 0, \\ & \frac{\partial}{\partial r}(r\beta u) + \frac{\partial}{\partial \theta}(\beta v) + \frac{\partial}{\partial s}(rw) = 0, \\ & \boldsymbol{\tau} + We \left(u \frac{\partial}{\partial r} + \frac{v}{r} \frac{\partial}{\partial \theta} + \frac{w}{\beta} \frac{\partial}{\partial s} \right) \boldsymbol{\tau} + We \frac{\partial \boldsymbol{\tau}}{\partial t} \\ & \quad = \frac{We}{r\beta} \mathbf{F}(\mathbf{u}, \boldsymbol{\tau}) + 2 \left(\varepsilon - \eta + \frac{\eta}{(r\beta)^{2q}} \left((r\beta)^2 + |r\beta D\mathbf{u}|^2 \right)^q \right) D\mathbf{u}, \\ & \mathbf{u}|_{\partial\Omega} = 0 \end{aligned} \right. \quad (3.1)$$

where for third-order tensor $\boldsymbol{\sigma}$, $\nabla \cdot \boldsymbol{\sigma}$ is given by

$$\begin{aligned}(\nabla \cdot \boldsymbol{\sigma})_r &= \frac{1}{r\beta} \left(\frac{\partial}{\partial r}(r\beta \sigma_{rr}) + \frac{\partial}{\partial \theta}(\beta \sigma_{r\theta}) + \frac{\partial}{\partial s}(r\sigma_{rs}) - \beta_2 \sigma_{ss} - \beta \sigma_{\theta\theta} \right), \\ (\nabla \cdot \boldsymbol{\sigma})_\theta &= \frac{1}{r\beta} \left(\frac{\partial}{\partial r}(r\beta \sigma_{\theta r}) + \frac{\partial}{\partial \theta}(\beta \sigma_{\theta\theta}) + \frac{\partial}{\partial s}(r\sigma_{\theta s}) + \beta_1 \sigma_{ss} + \beta \sigma_{r\theta} \right), \\ (\nabla \cdot \boldsymbol{\sigma})_s &= \frac{1}{r\beta} \left(\frac{\partial}{\partial r}(r\beta \sigma_{sr}) + \frac{\partial}{\partial \theta}(\beta \sigma_{s\theta}) + \frac{\partial}{\partial s}(r\sigma_{ss}) - \beta_1 \sigma_{\theta s} + \beta_2 \sigma_{rs} \right),\end{aligned}$$

and the velocity gradient and the symmetric tensor \mathbf{F} are given by

$$\begin{aligned}\nabla \mathbf{u} &= \begin{pmatrix} \frac{\partial u}{\partial r} & \frac{\partial v}{\partial r} & \frac{\partial w}{\partial r} \\ \frac{1}{r} \frac{\partial u}{\partial \theta} - \frac{v}{r} & \frac{1}{r} \frac{\partial v}{\partial \theta} + \frac{u}{r} & \frac{1}{r} \frac{\partial w}{\partial \theta} \\ \frac{1}{\beta} \frac{\partial u}{\partial s} - \frac{\beta_2}{r\beta} w & \frac{1}{\beta} \frac{\partial v}{\partial s} + \frac{\beta_1}{r\beta} w & \frac{1}{\beta} \frac{\partial w}{\partial s} + \frac{\beta_2}{r\beta} u - \frac{\beta_1}{r\beta} v \end{pmatrix}, \\ \mathbf{F}_{rr}(\mathbf{u}, \boldsymbol{\tau}) &= 2 \left(r\beta \frac{\partial u}{\partial r} \boldsymbol{\tau}_{rr} + \beta \frac{\partial u}{\partial \theta} \boldsymbol{\tau}_{r\theta} + r \frac{\partial u}{\partial s} \boldsymbol{\tau}_{rs} \right), \\ \mathbf{F}_{r\theta}(\mathbf{u}, \boldsymbol{\tau}) &= \beta \left(r \frac{\partial v}{\partial r} - v \right) \boldsymbol{\tau}_{rr} + \beta \left(\frac{\partial v}{\partial \theta} + u + r \frac{\partial u}{\partial r} \right) \boldsymbol{\tau}_{r\theta} \\ &\quad + r \frac{\partial v}{\partial s} \boldsymbol{\tau}_{rs} + \beta \frac{\partial u}{\partial \theta} \boldsymbol{\tau}_{\theta\theta} + r \frac{\partial u}{\partial s} \boldsymbol{\tau}_{\theta s}, \\ \mathbf{F}_{rs}(\mathbf{u}, \boldsymbol{\tau}) &= \left(r\beta \frac{\partial w}{\partial r} - \beta_2 w \right) \boldsymbol{\tau}_{rr} + \left(\beta \frac{\partial w}{\partial \theta} + \beta_1 w \right) \boldsymbol{\tau}_{r\theta} + \beta \frac{\partial u}{\partial \theta} \boldsymbol{\tau}_{\theta s} \\ &\quad + \left(r \frac{\partial w}{\partial s} + \beta_2 u - \beta_1 v + r\beta \frac{\partial u}{\partial r} \right) \boldsymbol{\tau}_{rs} + r \frac{\partial u}{\partial s} \boldsymbol{\tau}_{ss}, \\ \mathbf{F}_{\theta\theta}(\mathbf{u}, \boldsymbol{\tau}) &= 2 \left(\beta \left(r \frac{\partial v}{\partial r} - v \right) \boldsymbol{\tau}_{r\theta} + \beta \left(\frac{\partial v}{\partial \theta} + u \right) \boldsymbol{\tau}_{\theta\theta} + r \frac{\partial v}{\partial s} \boldsymbol{\tau}_{\theta s} \right),\end{aligned}$$

$$\begin{aligned}
\mathbf{F}_{\theta s}(\mathbf{u}, \boldsymbol{\tau}) &= \left(r\beta \frac{\partial w}{\partial r} - \beta_2 w\right) \boldsymbol{\tau}_{r\theta} + \left(\beta \frac{\partial w}{\partial \theta} + \beta_1 w\right) \boldsymbol{\tau}_{\theta\theta} + \beta \left(r \frac{\partial v}{\partial r} - v\right) \boldsymbol{\tau}_{rs} \\
&\quad + \left(r \frac{\partial w}{\partial s} + \beta_2 u - \beta_1 v + \beta \frac{\partial v}{\partial \theta} + \beta u\right) \boldsymbol{\tau}_{\theta s} + r \frac{\partial v}{\partial s} \boldsymbol{\tau}_{ss}, \\
\mathbf{F}_{ss}(\mathbf{u}, \boldsymbol{\tau}) &= 2 \left(\left(r\beta \frac{\partial w}{\partial r} - \beta_2 w\right) \boldsymbol{\tau}_{rs} + \left(\beta \frac{\partial w}{\partial \theta} + \beta_1 w\right) \boldsymbol{\tau}_{\theta s} \right) \\
&\quad + 2 \left(r \frac{\partial w}{\partial s} + \beta_2 u - \beta_1 v\right) \boldsymbol{\tau}_{ss}.
\end{aligned}$$

Considering fully developed flows, the velocity, the pressure and the stress tensor $\boldsymbol{\tau}$ are independent of the variable s . Consequently, they satisfy respectively,

$$\frac{\partial u}{\partial s} = \frac{\partial v}{\partial s} = \frac{\partial w}{\partial s} \equiv 0, \quad \frac{\partial p}{\partial s} = -p^* \quad \text{and} \quad \frac{\partial \hat{\boldsymbol{\tau}}}{\partial s} \equiv 0. \quad (3.2)$$

Using (3.2), problem (3.1) defined in the set

$$\Sigma = \{(r, \theta) \in \mathbb{R}^2 \mid 0 < r < 1, 0 < \theta \leq 2\pi\} \quad (3.3)$$

reads as follows

Find $(\mathbf{u} \equiv (u, v, w), p, \hat{\boldsymbol{\tau}})$ solution of

$$\mathcal{P} = \begin{cases} -\mathcal{A}_{r,\gamma} \left(\psi_\gamma (2(1-\varepsilon) D\mathbf{u} - \mathcal{R}e \mathbf{u} \otimes \mathbf{u}) + \hat{\boldsymbol{\tau}} \right) + \mathcal{R}e \frac{\partial u}{\partial t} + \psi_{\gamma+1} \frac{\partial p}{\partial r} = 0, \\ -\mathcal{A}_{\theta,\gamma} \left(\psi_\gamma (2(1-\varepsilon) D\mathbf{u} - \mathcal{R}e \mathbf{u} \otimes \mathbf{u}) + \hat{\boldsymbol{\tau}} \right) + \mathcal{R}e \frac{\partial v}{\partial t} + \beta \psi_\gamma \frac{\partial p}{\partial \theta} = 0, \\ -\mathcal{A}_{s,\gamma} \left(\psi_\gamma (2(1-\varepsilon) D\mathbf{u} - \mathcal{R}e \mathbf{u} \otimes \mathbf{u}) + \hat{\boldsymbol{\tau}} \right) + \mathcal{R}e \frac{\partial w}{\partial t} = p^* r \psi_\gamma, \\ \frac{\partial}{\partial r} (r\beta u) + \frac{\partial}{\partial \theta} (\beta v) = 0, \\ r\beta \hat{\boldsymbol{\tau}} + \mathcal{W}e \left(\frac{\partial}{\partial t} + r\beta u \frac{\partial}{\partial r} + \beta v \frac{\partial}{\partial \theta} \right) \hat{\boldsymbol{\tau}} = \mathbf{G}(\mathbf{u}, \hat{\boldsymbol{\tau}}) \\ \mathbf{u}|_{\partial\Sigma} = 0 \end{cases} \quad (3.4)$$

where for a tensor σ ,

$$\mathcal{A}_{\xi,\gamma}(\boldsymbol{\sigma}) = r\beta(\nabla \cdot \boldsymbol{\sigma})_\xi - \gamma((\beta + \beta_2)\boldsymbol{\sigma}_{\xi r} - \beta_1 \boldsymbol{\sigma}_{\xi \theta}), \quad \text{for any } \xi = r, \theta, s$$

and

$$\begin{aligned}
\mathbf{G}(\mathbf{u}, \hat{\boldsymbol{\tau}}) &= \mathcal{W}e \left(\mathbf{F}(\mathbf{u}, \hat{\boldsymbol{\tau}}) + \gamma((\beta + \beta_2)u - \beta_1 v) \hat{\boldsymbol{\tau}} \right) \\
&\quad + 2(\varepsilon - \eta) \psi_\gamma D\mathbf{u} \\
&\quad + 2\eta \psi_{\gamma-2q+1} \left((r\beta)^2 + |r\beta D\mathbf{u}|^2 \right)^q D\mathbf{u},
\end{aligned} \quad (3.5)$$

where $\gamma = 2 \max(q, 0) + 1$, $\psi_\gamma = (r\beta)^\gamma$ and $\hat{\boldsymbol{\tau}} \equiv \psi_\gamma \boldsymbol{\tau}$.

4. Numerical approximation and results

We use finite element methods to obtain approximate solutions to problem (3.4). Here and in the remaining sections, only steady solutions will be considered.

4.1. Setting of the approximated problem

Let $\{\mathcal{T}_h\}_{h>0}$ be a family of regular triangulations of the rectangle Σ defined by (3.3), and denote by

$$\begin{aligned}\mathbf{X}_h &= (X_h)^3 = \left\{ \mathbf{v}_h \in \mathbf{C}(\bar{\Sigma}) \cap \mathbf{H}_0^1(\Sigma) \mid \mathbf{v}_h|_K \in \mathbb{P}_2(K), \forall K \in \mathcal{T}_h \right\}^3, \\ Q_h &= \left\{ q_h \in C(\bar{\Sigma}) \cap L_0^2(\Sigma) \mid q_h|_K \in \mathbb{P}_1(K), \forall K \in \mathcal{T}_h \right\},\end{aligned}$$

and

$$\mathbf{T}_h = (T_h)^{3 \times 3} = \left\{ \tau_h \in L^2(\Sigma) \mid \tau_h|_K \in \mathbb{P}_1, \forall K \in \mathcal{T}_h \right\}^{3 \times 3}$$

the finite element spaces. System (3.4) is approximated by the following problem

Find $(\mathbf{u}_h, p_h, \hat{\boldsymbol{\tau}}_h) \equiv (\mathbf{u}, p, \hat{\boldsymbol{\tau}}) \in \mathbf{X}_h \times Q_h \times \mathbf{T}_h$ solution of

$$\left\{ \begin{array}{l} \left(-\mathcal{A}_{r,\gamma}(\psi_\gamma(2(1-\varepsilon)D\mathbf{u} - \mathcal{R}e \mathbf{u} \otimes \mathbf{u})) + \psi_{\gamma+1} \frac{\partial p}{\partial r}, \phi_1 \right) = (\mathcal{A}_{r,\gamma}(\hat{\boldsymbol{\tau}}), \phi_1), \\ \left(-\mathcal{A}_{\theta,\gamma}(\psi_\gamma(2(1-\varepsilon)D\mathbf{u} - \mathcal{R}e \mathbf{u} \otimes \mathbf{u})) + \beta \psi_\gamma \frac{\partial p}{\partial \theta}, \phi_2 \right) = (\mathcal{A}_{\theta,\gamma}(\hat{\boldsymbol{\tau}}), \phi_2), \\ \left(-\mathcal{A}_{s,\gamma}(\psi_\gamma(2(1-\varepsilon)D\mathbf{u} - \mathcal{R}e \mathbf{u} \otimes \mathbf{u})) - p^* r \psi_\gamma, \phi_3 \right) = (\mathcal{A}_{s,\gamma}(\hat{\boldsymbol{\tau}}), \phi_3), \\ \left(\frac{\partial}{\partial r}(r\beta u) + \frac{\partial}{\partial \theta}(\beta v), \varphi \right) = 0, \\ \left(r\beta \hat{\boldsymbol{\tau}}_{ij}, \boldsymbol{\sigma}_\ell \right) + \mathcal{W}e \mathcal{B}_h(u, v, \hat{\boldsymbol{\tau}}_{ij}, \boldsymbol{\sigma}_\ell) = \left(\mathbf{G}_{ij}(\mathbf{u}, \hat{\boldsymbol{\tau}}), \boldsymbol{\sigma}_\ell \right), \\ \mathbf{u}|_{\partial\Sigma} = 0 \end{array} \right. \quad (4.1)$$

for every $(\phi_1, \phi_2, \phi_3, \varphi) \in \mathbf{V}_{\delta,h} \times Q_h$, where

$$\mathbf{V}_{\delta,h} = \{ \mathbf{v}_h \in \mathbf{X}_h \mid \nabla' \cdot (\beta \mathbf{v}_h) = 0 \}, \quad \delta \in [0, 1[$$

and every $\boldsymbol{\sigma}_\ell \in T_h$ ($\ell = 1, \dots, 6$), with \mathcal{B}_h defined by

$$\begin{aligned}\mathcal{B}_h(u, v, \tau, \sigma) &= \left(r\beta u \frac{\partial \tau}{\partial r} + \beta v \frac{\partial \tau}{\partial \theta} + \frac{1}{2} \left(\frac{\partial}{\partial r}(r\beta u) + \frac{\partial}{\partial \theta}(\beta v) \right) \tau, \sigma \right)_h \\ &\quad - \langle \tau^+ - \tau^-, \sigma^+ \rangle_{h,u,v}\end{aligned}$$

where

$$(\cdot, \cdot)_h = \sum_{K \in \mathcal{T}_h} (\cdot, \cdot)_K,$$

$$\langle \sigma, \tau \rangle_{h,u,v} = \sum_{K \in \mathcal{T}_h} \int_{\partial K^-(ru,v)} \tau \sigma \beta (run_r + vn_\theta) ds,$$

$$\partial K^-(\psi, \zeta) = \{ s \in \partial K \mid (\psi, \zeta) \cdot (n_r, n_\theta) < 0 \},$$

and where (n_r, n_θ) is the outward unit normal vector to element $K \in \mathcal{T}_h$.

Using standard integration by parts we show that problem (4.1) can be rewritten in the form

(\mathcal{P}_h) Find $(\mathbf{u}_h, p_h, \hat{\boldsymbol{\tau}}_h) \equiv (\mathbf{u}, p, \hat{\boldsymbol{\tau}}) \in \mathbf{X}_h \times Q_h \times \mathbf{T}_h$ solution of

$$\begin{aligned} & 2\mathcal{K}_\gamma\left(\psi_\gamma \frac{\partial u}{\partial r}, \phi_1\right) + \mathcal{L}_\gamma\left(\beta\psi_{\gamma-1} \frac{\partial u}{\partial \theta}, \phi_1\right) + 2\left(\psi_{\gamma-1} (\beta^2 + \beta_2^2) u, \phi_1\right) \\ & + \mathcal{L}_\gamma\left(\beta\psi_{\gamma-1} \left(r \frac{\partial v}{\partial r} - v\right), \phi_1\right) + 2\left(\psi_{\gamma-1} \left(\beta^2 \frac{\partial v}{\partial \theta} - \beta_1 \beta_2 v\right), \phi_1\right) \\ & - \frac{1}{1-\varepsilon} \mathcal{K}_{\gamma+1}\left(\psi_\gamma p, \phi_1\right) + \frac{\mathcal{R}e}{1-\varepsilon} \left(\mathcal{K}_\gamma\left(\psi_\gamma u^2, \phi_1\right) + \mathcal{L}_\gamma\left(\psi_\gamma uv, \phi_1\right)\right) \\ & + \frac{\mathcal{R}e}{1-\varepsilon} \left(\psi_\gamma (\beta_2 w^2 + \beta v^2), \phi_1\right) \\ & = -\frac{1}{1-\varepsilon} \left(\mathcal{K}_\gamma(\hat{\boldsymbol{\tau}}_{rr}, \phi_1) + \mathcal{L}_\gamma(\hat{\boldsymbol{\tau}}_{r\theta}, \phi_1) + (\beta_2 \hat{\boldsymbol{\tau}}_{ss} + \beta \hat{\boldsymbol{\tau}}_{\theta\theta}, \phi_1)\right), \end{aligned}$$

$$\begin{aligned} & \mathcal{K}_\gamma\left(\beta\psi_{\gamma-1} \left(r \frac{\partial v}{\partial r} - v\right), \phi_2\right) + 2\mathcal{L}_\gamma\left(\beta\psi_{\gamma-1} \frac{\partial v}{\partial \theta}, \phi_2\right) \\ & + \left(\psi_{\gamma-1} \left((\beta^2 + 2\beta_1^2) v - r\beta^2 \frac{\partial v}{\partial r}\right), \phi_2\right) + \mathcal{K}_\gamma\left(\beta\psi_{\gamma-1} \frac{\partial u}{\partial \theta}, \phi_2\right) \\ & + 2\mathcal{L}_\gamma\left(\beta\psi_{\gamma-1} u, \phi_2\right) - \left(\psi_{\gamma-1} \left(\beta^2 \frac{\partial u}{\partial \theta} + 2\beta_1 \beta_2 u\right), \phi_2\right) \\ & - \frac{1}{1-\varepsilon} \mathcal{L}_{\gamma+1}\left(\psi_\gamma p, \phi_2\right) + \frac{\mathcal{R}e}{1-\varepsilon} \left(\mathcal{K}_\gamma\left(\psi_\gamma uv, \phi_2\right) + \mathcal{L}_\gamma\left(\psi_\gamma v^2, \phi_2\right)\right) \\ & - \frac{\mathcal{R}e}{1-\varepsilon} \left(\psi_\gamma (\beta_1 w^2 + \beta uv), \phi_2\right) \\ & = -\frac{1}{1-\varepsilon} \left(\mathcal{K}_\gamma(\hat{\boldsymbol{\tau}}_{\theta r}, \phi_2) + \mathcal{L}_\gamma(\hat{\boldsymbol{\tau}}_{\theta\theta}, \phi_2) - (\beta_1 \hat{\boldsymbol{\tau}}_{ss} + \beta \hat{\boldsymbol{\tau}}_{r\theta}, \phi_2)\right), \end{aligned}$$

$$\begin{aligned} & \mathcal{K}_\gamma\left(\psi_{\gamma-1} \left(r\beta \frac{\partial w}{\partial r} - \beta_2 w\right), \phi_3\right) + \mathcal{L}_\gamma\left(\psi_{\gamma-1} \left(\beta \frac{\partial w}{\partial \theta} + \beta_1 w\right), \phi_3\right) \\ & + \left(\psi_{\gamma-1} \left((r\delta)^2 w + \beta\beta_1 \frac{\partial w}{\partial \theta} - r\beta\beta_2 \frac{\partial w}{\partial r}\right), \phi_3\right) \\ & - \frac{1}{1-\varepsilon} \left(r\psi_\gamma p^*, \phi_3\right) + \frac{\mathcal{R}e}{1-\varepsilon} \left(\mathcal{K}_\gamma\left(\psi_\gamma uw, \phi_3\right) + \mathcal{L}_\gamma\left(\psi_\gamma vw, \phi_3\right)\right) \\ & - \frac{\mathcal{R}e}{1-\varepsilon} \left(\psi_\gamma (\beta_2 u - \beta_1 v) w, \phi_3\right) \\ & = -\frac{1}{1-\varepsilon} \left(\mathcal{K}_\gamma(\hat{\boldsymbol{\tau}}_{sr}, \phi_3) + \mathcal{L}_\gamma(\hat{\boldsymbol{\tau}}_{s\theta}, \phi_3) + (\beta_1 \hat{\boldsymbol{\tau}}_{\theta s} - \beta_2 \hat{\boldsymbol{\tau}}_{rs}, \phi_3)\right), \end{aligned}$$

$$\left(\frac{\partial}{\partial r} (r\beta u) + \frac{\partial}{\partial \theta} (\beta v), \varphi\right) = 0, \text{ for every } (\phi_1, \phi_2, \phi_3, \varphi) \in \mathbf{V}_{\delta,h} \times Q_h, \text{ and}$$

$$(\hat{\boldsymbol{\tau}}_{ij}, r\beta\boldsymbol{\sigma}_\ell)_h + \mathcal{W}e \mathcal{B}_h(u, v, \hat{\boldsymbol{\tau}}_{ij}, \boldsymbol{\sigma}_\ell) = (\mathbf{G}_{ij}(\mathbf{u}, \hat{\boldsymbol{\tau}}), \boldsymbol{\sigma}_\ell)_h$$

for all $\boldsymbol{\sigma} \in (T_h)^6$ with

$$\mathcal{B}_h = -\left(r\beta u \frac{\partial \sigma}{\partial r} + \beta v \frac{\partial \sigma}{\partial \theta} - \frac{1}{2} \left(\frac{\partial}{\partial r} (r\beta u) + \frac{\partial}{\partial \theta} (\beta v)\right) \sigma, \tau\right)_h + \langle \tau^-, \sigma^+ - \sigma^- \rangle_{h,u,v},$$

with $\mathcal{K}_\gamma(\sigma, \varphi) = \left(\sigma, r\beta \frac{\partial \varphi}{\partial r} + \gamma(\beta + \beta_2) \varphi\right)$, $\mathcal{L}_\gamma(\sigma, \varphi) = \left(\sigma, \beta \frac{\partial \varphi}{\partial \theta} - \gamma\beta_1 \varphi\right)$ and \mathbf{G} given by (3.5).

4.2. Algorithm

Next we define the algorithm to solve the approximated problem (\mathcal{P}_h) (as usual, the index h is dropped to simplify the presentation).

- Given an iterate $\hat{\boldsymbol{\tau}}^k$, find $\mathbf{u}^k \equiv (u^k, v^k, w^k)$, and p^k solutions of the following Navier-Stokes system $(NS)_k$

$$\begin{aligned} & 2\mathcal{K}_\gamma \left(\psi_\gamma \frac{\partial u^k}{\partial r}, \phi_1 \right) + \mathcal{L}_\gamma \left(\beta \psi_{\gamma-1} \frac{\partial u^k}{\partial \theta}, \phi_1 \right) + 2 \left(\psi_{\gamma-1} (\beta^2 + \beta_2^2) u^k, \phi_1 \right) \\ & + \mathcal{L}_\gamma \left(\beta \psi_{\gamma-1} \left(r \frac{\partial v^k}{\partial r} - v^k \right), \phi_1 \right) + 2 \left(\psi_{\gamma-1} \left(\beta^2 \frac{\partial v^k}{\partial \theta} - \beta_1 \beta_2 v^k \right), \phi_1 \right) \\ & - \frac{1}{1-\varepsilon} \mathcal{K}_{\gamma+1} \left(\psi_\gamma p^k, \phi_1 \right) + \frac{\mathcal{R}e}{1-\varepsilon} \mathcal{K}_\gamma \left(\psi_\gamma (u^k)^2, \phi_1 \right) \\ & + \frac{\mathcal{R}e}{1-\varepsilon} \left(\mathcal{L}_\gamma \left(\psi_\gamma u^k v^k, \phi_1 \right) + \left(\psi_\gamma (\beta_2 (w^k)^2 + \beta (v^k)^2), \phi_1 \right) \right) \\ & = - \frac{1}{1-\varepsilon} \left(\mathcal{K}_\gamma (\hat{\boldsymbol{\tau}}_{rr}^k, \phi_1) + \mathcal{L}_\gamma (\hat{\boldsymbol{\tau}}_{r\theta}^k, \phi_1) + (\beta_2 \hat{\boldsymbol{\tau}}_{ss}^k + \beta \hat{\boldsymbol{\tau}}_{\theta\theta}^k, \phi_1) \right), \end{aligned}$$

$$\begin{aligned} & \mathcal{K}_\gamma \left(\beta \psi_{\gamma-1} \left(r \frac{\partial v^k}{\partial r} - v^k \right), \phi_2 \right) + 2\mathcal{L}_\gamma \left(\beta \psi_{\gamma-1} \frac{\partial v^k}{\partial \theta}, \phi_2 \right) \\ & + \left(\psi_{\gamma-1} \left((\beta^2 + 2\beta_1^2) v^k - r \beta^2 \frac{\partial v^k}{\partial r} \right), \phi_2 \right) + \mathcal{K}_\gamma \left(\beta \psi_{\gamma-1} \frac{\partial u^k}{\partial \theta}, \phi_2 \right) \\ & + 2\mathcal{L}_\gamma \left(\beta \psi_{\gamma-1} u^k, \phi_2 \right) - \left(\psi_{\gamma-1} \left(\beta^2 \frac{\partial u^k}{\partial \theta} + 2\beta_1 \beta_2 u^k \right), \phi_2 \right) \\ & - \frac{1}{1-\varepsilon} \mathcal{L}_{\gamma+1} \left(\psi_\gamma p^k, \phi_2 \right) + \frac{\mathcal{R}e}{1-\varepsilon} \mathcal{K}_\gamma \left(\psi_\gamma u^k v^k, \phi_2 \right) \\ & + \frac{\mathcal{R}e}{1-\varepsilon} \left(\mathcal{L}_\gamma \left(\psi_\gamma (v^k)^2, \phi_2 \right) - \left(\psi_\gamma (\beta_1 (w^k)^2 + \beta u^k v^k), \phi_2 \right) \right) \\ & = - \frac{1}{1-\varepsilon} \left(\mathcal{K}_\gamma (\hat{\boldsymbol{\tau}}_{\theta r}^k, \phi_2) + \mathcal{L}_\gamma (\hat{\boldsymbol{\tau}}_{\theta\theta}^k, \phi_2) - (\beta_1 \hat{\boldsymbol{\tau}}_{ss}^k + \beta \hat{\boldsymbol{\tau}}_{r\theta}^k, \phi_2) \right), \end{aligned}$$

$$\begin{aligned} & \mathcal{K}_\gamma \left(\psi_{\gamma-1} \left(r \beta \frac{\partial w^k}{\partial r} - \beta_2 w^k \right), \phi_3 \right) + \mathcal{L}_\gamma \left(\psi_{\gamma-1} \left(\beta \frac{\partial w^k}{\partial \theta} + \beta_1 w^k \right), \phi_3 \right) \\ & + \left(\psi_{\gamma-1} \left((r\delta)^2 w^k + \beta \beta_1 \frac{\partial w^k}{\partial \theta} - r \beta \beta_2 \frac{\partial w^k}{\partial r} \right), \phi_3 \right) \\ & - \frac{1}{1-\varepsilon} \left(r \psi_\gamma p^*, \phi_3 \right) + \frac{\mathcal{R}e}{1-\varepsilon} \mathcal{K}_\gamma \left(\psi_\gamma u^k w^k, \phi_3 \right) \\ & + \frac{\mathcal{R}e}{1-\varepsilon} \left(\mathcal{L}_\gamma \left(\psi_\gamma v^k w^k, \phi_3 \right) - \left(\psi_\gamma (\beta_2 u^k - \beta_1 v^k) w^k, \phi_3 \right) \right) \\ & = - \frac{1}{1-\varepsilon} \left(\mathcal{K}_\gamma (\hat{\boldsymbol{\tau}}_{sr}^k, \phi_3) + \mathcal{L}_\gamma (\hat{\boldsymbol{\tau}}_{s\theta}^k, \phi_3) + (\beta_1 \hat{\boldsymbol{\tau}}_{\theta s}^k - \beta_2 \hat{\boldsymbol{\tau}}_{rs}^k, \phi_3) \right), \end{aligned}$$

$$\left(\frac{\partial}{\partial r} (r \beta u^k) + \frac{\partial}{\partial \theta} (\beta v^k), \varphi \right) = 0, \text{ for every } (\phi_1, \phi_2, \phi_3, \varphi) \in \mathbf{V}_{\delta, \mathbf{h}} \times \mathbf{Q}_{\mathbf{h}}.$$

- Calculate the new iterate $\hat{\boldsymbol{\tau}}^{k+1}$ as the solution of the transport problem $\left(\hat{\boldsymbol{\tau}}_{ij}^{k+1}, r \beta \boldsymbol{\sigma}_\ell \right) + \mathcal{W}e \mathcal{B}_h \left(u^k, v^k, \hat{\boldsymbol{\tau}}_{ij}^{k+1}, \boldsymbol{\sigma}_\ell \right) = \left(\mathbf{G}_{ij}(\mathbf{u}^k, \hat{\boldsymbol{\tau}}^k), \boldsymbol{\sigma}_\ell \right) \quad \forall \boldsymbol{\sigma} \in (T_h)^6.$
- Find $\mathbf{u}^{k+1} \equiv (u^{k+1}, v^{k+1}, w^{k+1}, p^{k+1})$ solution of the Navier-Stokes system $(NS)_{k+1}$.

Taking into account this algorithm, our aim is to write the linear systems corresponding to problem (\mathcal{P}_h) at a given iteration k . To simplify the presentation, we will consider the case of creeping non-Newtonian flows, which corresponds to $\mathcal{R}e = 0$.

Given $\hat{\tau}^k$, expressing the corresponding approximate solutions u^k , v^k , w^k and p^k in the basis of $\mathbf{V}_{\delta, \mathbf{h}}$ and Q_h

$$u^k = \sum_{i=1}^{n_h} u_i^k \phi_1^i, \quad v^k = \sum_{i=1}^{n_h} v_i^k \phi_2^i, \quad w^k = \sum_{i=1}^{n_h} w_i^k \phi_3^i, \quad p^k = \sum_{i=1}^{m_h} p_i^k \varphi^i,$$

we obtain the following linear system

$$\begin{pmatrix} \mathbf{A}_1 & \mathbf{A}_2 & 0 & \frac{1}{1-\varepsilon} \mathbf{A}_3 \\ \mathbf{A}_4 & \mathbf{A}_5 & 0 & \frac{1}{1-\varepsilon} \mathbf{A}_6 \\ 0 & 0 & \mathbf{A}_7 & 0 \\ \mathbf{A}_8 & \mathbf{A}_9 & 0 & 0 \end{pmatrix} \begin{pmatrix} u^k \\ v^k \\ w^k \\ p^k \end{pmatrix} = \begin{pmatrix} \mathbf{b}_1^k \\ \mathbf{b}_2^k \\ \mathbf{b}_3^k \\ 0 \end{pmatrix}$$

where

$$(\mathbf{A}_1)_{ij} = 2\mathcal{K}_\gamma \left(\psi_\gamma \frac{\partial \phi_1^j}{\partial r}, \phi_1^i \right) + \mathcal{L}_\gamma \left(\beta \psi_{\gamma-1} \frac{\partial \phi_1^j}{\partial \theta}, \phi_1^i \right) + 2 \left(\psi_{\gamma-1} (\beta^2 + \beta_2^2) \phi_1^j, \phi_1^i \right),$$

$$(\mathbf{A}_2)_{ij} = \mathcal{L}_\gamma \left(\psi_{\gamma-1} \left(r \beta \frac{\partial \phi_2^j}{\partial r} - \beta \phi_2^j \right), \phi_1^i \right) + 2 \left(\psi_{\gamma-1} \left(\beta^2 \frac{\partial \phi_2^j}{\partial \theta} - \beta_1 \beta_2 \phi_2^j \right), \phi_1^i \right),$$

$$(\mathbf{A}_3)_{ij} = -\mathcal{K}_{\gamma+1} \left(\psi_\gamma \varphi^j, \phi_1^i \right),$$

$$(\mathbf{A}_4)_{ij} = \mathcal{K}_\gamma \left(\beta \psi_{\gamma-1} \frac{\partial \phi_1^j}{\partial \theta}, \phi_2^i \right) + 2\mathcal{L}_\gamma \left(\beta \psi_{\gamma-1} \phi_1^j, \phi_2^i \right) - \left(\psi_{\gamma-1} \left(\beta^2 \frac{\partial \phi_1^j}{\partial \theta} + 2\beta_1 \beta_2 \phi_1^j \right), \phi_2^i \right),$$

$$(\mathbf{A}_5)_{ij} = \mathcal{K}_\gamma \left(\psi_{\gamma-1} \left(r \beta \frac{\partial \phi_2^j}{\partial r} - \beta \phi_2^j \right), \phi_2^i \right) + 2\mathcal{L}_\gamma \left(\beta \psi_{\gamma-1} \frac{\partial \phi_2^j}{\partial \theta}, \phi_2^i \right) + \left(\psi_{\gamma-1} \left((\beta^2 + 2\beta_1^2) \phi_2^j - r \beta^2 \frac{\partial \phi_2^j}{\partial r} \right), \phi_2^i \right),$$

$$(\mathbf{A}_6)_{ij} = -\mathcal{L}_{\gamma+1} \left(\psi_\gamma \varphi^j, \phi_2^i \right),$$

$$(\mathbf{A}_7)_{ij} = \mathcal{K}_\gamma \left(\psi_{\gamma-1} \left(r \beta \frac{\partial \phi_3^j}{\partial r} - \beta_2 \phi_3^j \right), \phi_3^i \right) + \mathcal{L}_\gamma \left(\psi_{\gamma-1} \left(\beta \frac{\partial \phi_3^j}{\partial \theta} + \beta_1 \phi_3^j \right), \phi_3^i \right) + \left(\psi_{\gamma-1} \left((r\delta)^2 \phi_3^j + \beta \beta_1 \frac{\partial \phi_3^j}{\partial \theta} - r \beta \beta_2 \frac{\partial \phi_3^j}{\partial r} \right), \phi_3^i \right),$$

$$(\mathbf{A}_8)_{ij} = \left(r \beta \frac{\partial \phi_1^j}{\partial r} + (\beta + \beta_2) \phi_1^j, \varphi^j \right),$$

$$(\mathbf{A}_9)_{ij} = \left(\beta \frac{\partial \phi_2^j}{\partial \theta} - \beta_1 \phi_2^j, \varphi^j \right),$$

and where the vectors \mathbf{b}_j ($j = 1, 3$) are given by

$$(\mathbf{b}_1^k)_i = -\frac{1}{1-\varepsilon} \left(\mathcal{K}_\gamma(\hat{\tau}_{rr}^k, \phi_1^i) + \mathcal{L}_\gamma(\hat{\tau}_{r\theta}^k, \phi_1^i) + (\beta_2 \hat{\tau}_{ss}^k + \beta \hat{\tau}_{\theta\theta}^k, \phi_1^i) \right),$$

$$(\mathbf{b}_2^k)_i = -\frac{1}{1-\varepsilon} \left(\mathcal{K}_\gamma(\hat{\tau}_{\theta r}^k, \phi_2^i) + \mathcal{L}_\gamma(\hat{\tau}_{\theta\theta}^k, \phi_2^i) - (\beta_1 \hat{\tau}_{ss}^k + \beta \hat{\tau}_{r\theta}^k, \phi_2^i) \right),$$

$$\begin{aligned}
(\mathbf{b}_3^k)_i = & -\frac{1}{1-\varepsilon} \left(\mathcal{K}_\gamma(\hat{\boldsymbol{\tau}}_{sr}^k, \phi_3^i) + \mathcal{L}_\gamma(\hat{\boldsymbol{\tau}}_{s\theta}^k, \phi_3^i) + (\beta_1 \hat{\boldsymbol{\tau}}_{\theta s}^k - \beta_2 \hat{\boldsymbol{\tau}}_{rs}^k, \phi_3^i) \right) \\
& + \frac{1}{1-\varepsilon} \left(r\psi_\gamma p^*, \phi_3^i \right).
\end{aligned}$$

After obtaining (u^k, v^k, w^k, p^k) , we consider the transport equation to get $\hat{\boldsymbol{\tau}}^{k+1} \equiv (\hat{\boldsymbol{\tau}}_{ij}^{k+1})$. Using the local basis functions $\{\zeta_\ell\}_{\ell=1,2,3} \subset T_h$, the local system for the approximate transport problem can be written as

$$\mathbf{A}^k \boldsymbol{\tau}_{ij}^{k+1} + (\mathbf{A}^k)^- (\boldsymbol{\tau}_{ij}^{k+1})^- = \mathbf{G}_{ij}^k, \quad i, j = 1, 2, 3$$

with

$$\begin{aligned}
\mathbf{A}_{\ell m}^k = & \left(\zeta_m, r\beta \zeta_l \right)_K - \mathcal{W}e \left(\zeta_m, r\beta u^k \frac{\partial \zeta_l}{\partial r} + \beta v^k \frac{\partial \zeta_l}{\partial \theta} \right)_K \\
& - \frac{\mathcal{W}e}{2} \left(\left(r\beta \frac{\partial u^k}{\partial r} + \beta \frac{\partial v^k}{\partial \theta} + (\beta + \beta_2)u^k - \beta_1 v^k \right) \zeta_m, \zeta_l \right)_K, \\
(\mathbf{A}^k)_{\ell m}^- = & \mathcal{W}e \int_{\partial K^-(ru_h, v_h)} \beta \zeta_m^- (\zeta_l - \zeta_l^-) (ru^k nr + v^k n_\theta) ds, \\
(\mathbf{G}_{ij}^k)_\ell = & \left(\mathbf{G}_{ij}(\mathbf{u}^k, \hat{\boldsymbol{\tau}}^k), \zeta_\ell \right)_K,
\end{aligned}$$

where ζ_ℓ^- denotes the ℓ th basis function over the correspondent adjacent element to K by an inflow edge, \mathbf{G} is the function given by (3.5). The local systems lead to a linear system of the form

$$M^k \boldsymbol{\tau}_i^{k+1} = \mathbf{C}_i^k,$$

where M^k is a non-symmetric matrix whose dimension is twice the number of nodes in the triangulation.

4.3. Numerical results

The domain Σ defined by (3.3) is discretized using triangles. Referring to the algorithm, we see that a Navier-Stokes system has to be solved for (u, v, p) , a Poisson equation for w and a transport equation for $\hat{\boldsymbol{\tau}}$. The velocity is set to zero on the lateral surface of the pipe. The non-dimensional stream function ψ can be written with respect to the components u and v , as

$$u = -\frac{1}{r\beta} \frac{\partial \psi}{\partial \theta}, \quad v = \frac{1}{\beta} \frac{\partial \psi}{\partial r}.$$

and the wall-shear stress is $\boldsymbol{\tau}_w = -(\mathbf{T} \cdot \mathbf{n}) \cdot \boldsymbol{\lambda}|_{r=1}$. In this particular case, $\boldsymbol{\tau}_w$ is given by

$$\begin{aligned}
\boldsymbol{\tau}_w = & -2(1-\varepsilon) \left(\frac{\partial u}{\partial r} - \left(\frac{\partial v}{\partial \theta} + u \right) \right) \Big|_{r=1} \sin \theta \cos \theta \\
& - (1-\varepsilon) \left(\frac{\partial v}{\partial r} + \left(\frac{\partial u}{\partial \theta} - v \right) \right) \Big|_{r=1} (\sin^2 \theta - \cos^2 \theta) \\
& - (\boldsymbol{\tau}_{rr} - \boldsymbol{\tau}_{\theta\theta}) \Big|_{r=1} \sin \theta \cos \theta - \boldsymbol{\tau}_{r\theta} \Big|_{r=1} (\sin^2 \theta - \cos^2 \theta).
\end{aligned}$$

In what follows, we consider the numerical simulation of fully developed steady Oldroyd-B flows with constant and non constant viscosity, in a curved pipe with constant cross section. The behavior of creeping (i.e., Reynolds number

set to zero) and inertial flows (non-zero Reynolds number) is analyzed for different values of the parameter involved in the governing equations (the Reynolds number \mathcal{Re} , the Weissenberg number \mathcal{We} , the curvature ration δ , the non-dimensional viscosity parameter η and the exponent q appearing in the power-law type viscosity). A continuation method is carried out to implement these different tests.

4.3.1. Creeping generalized Oldroyd-B flows. In this section, we are interested in the qualitative study of creeping flows ($\mathcal{Re} = 0$) for generalized Oldroyd-B fluids, and especially on the behavior of the secondary motions and of the wall shear stress. In order to analyse the combined effect of the viscoelasticity, the non-constant viscosity and the curvature ratio, several calculations were achieved.

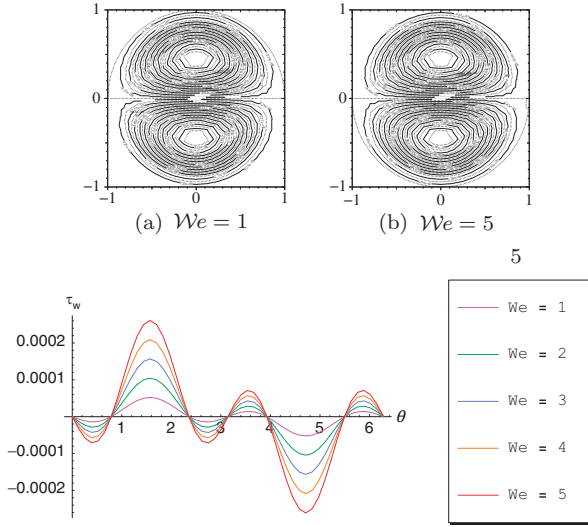


FIGURE 2. Streamlines (top) and wall shear stress (bottom) for creeping Oldroyd-B flows, for the curvature ratio $\delta = 0.001$.

It is well known that in the case of creeping Oldroyd-B fluids, the viscoelasticity promotes secondary flows characterized by two counter-rotating vortices, that the global behavior is stable, and is of Newtonian type. We did not observe any notable changes in the nature of the flow when varying the characteristic parameters (Weissenberg number and curvature ratio). The only difference lies in the values of the stream function and of the wall shear stress, which increase with these parameters, and also in a slight shift to the left of the vortices with increasing curvature ratio. Figure 2 displays the flow behavior for the curvature ratio $\delta = 0.001$.

In a second step, we consider the more general case of Oldroyd-B fluids with non constant viscosity. Fixing the curvature ratio δ and the viscosity parameter η , we implement a continuation method with respect to the exponent q , for different

values of the Weissenberg number. The values of the maximum exponent for which convergence is ensured are shown in Table 1. As one can see, and as expected, q_{max} depends on the different parameters. In particular, the values decrease when these parameters increase. We also observe that there is no convergence, for the curvature ratio $\delta = 0.2$, with $We = 5$ and the same values of the viscosity parameter η .

We	1	2	3	4	5
$\delta = 0.001$					
$\eta = 0.4$	21.6	6.80	6.75	7.32	6.93
0.5	4.70	4.57	4.45	4.15	3.95
0.6	3.05	2.85	2.60	2.30	2.00
$\delta = 0.1$					
$\eta = 0.4$	8.92	1.02	0.58	0.45	0.36
0.5	1.53	0.60	0.42	0.32	0.26
0.6	0.80	0.45	0.32	0.26	0.21
$\delta = 0.2$					
$\eta = 0.4$	3.31	0.62	0.42	0.32	—
0.5	0.91	0.45	0.32	0.24	—
0.6	0.60	0.34	0.24	0.19	—

TABLE 1. Maximum values of $|q|$.

Numerical results (using finite element methods) show some changes in flow characteristics and that the viscosity influences its behavior. In summary, we have two phases:

- A phase of variation in the behavior passing from the standard Oldroyd-B type to a new type.
- A phase of stabilisation in the new type.

More precisely, for small values of $|q|$, we observe a surprising phenomenon. Initially, the secondary flows involve non-zero values and are characterized by two counter-rotating vortices. As q increases in absolute value, the streamlines in the core region become less dense, the size of the couple of vortices reduces, and the flow is driven near the wall pipe. We observe the formation of boundary layers flows with a pair of new vortices, initially weak and elongated, strengthening and dominating as the viscosity exponent increases. In contrast, the original secondary flows become more and more weak before vanishing when the level of the exponent viscosity reaches a critical value. The orientation of the new contours is opposite, as well as the sign of the stream function, suggesting a *transition* to a different regime.

It is interesting to observe that this behavior is global, in the sense that it is seems to be independent of the Weissenberg number and of the curvature ratio, and occurs for the same values of the viscosity exponent q . Figure 3 illustrates the behavior of the streamlines in the particular case of a curvature ratio $\delta = 0.001$ and

viscosity parameter $\eta = 0.4$. The influence of the viscosity parameter is evident, and as η increases the transition occurs earlier. Moreover, because of the effect of the curvature, the new two vortices are not localized in the center of the cross section but are slightly translated.

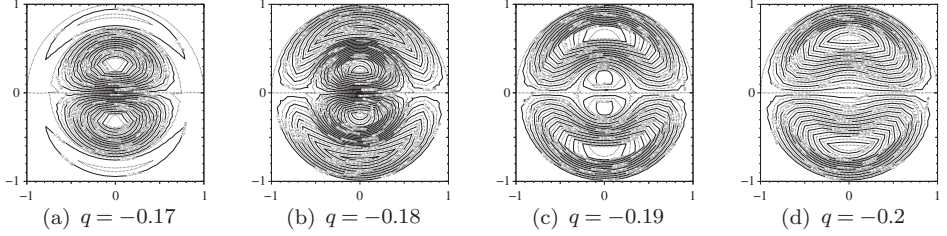


FIGURE 3. Qualitative behavior of the streamlines for creeping generalized Oldroyd-B flows, with $\eta=0.4$ and for different values of $|q|$ ($\delta=0.001$).

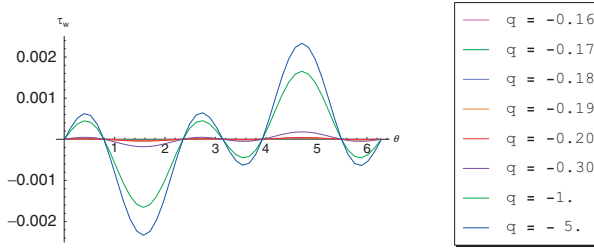


FIGURE 4. Wall shear stress for creeping generalized Oldroyd-B flows, with $\eta=0.4$ ($\delta=0.001$).

We also noticed variations in the wall shear stress (see [Figure 4](#)). It can be observed that during the *transition*, the amplitude of the wall shear stress decreases and the corresponding curves are inverted in comparison with the Oldroyd-B case.

After the transition phase, and before reaching some “critical” value of the viscosity exponent, the flow is qualitatively more stable. The streamlines are symmetric and the global behavior of the wall shear stress remains unchanged. This critical value of q depends on the viscoelastic parameter, on the viscosity parameter, and particularly on the curvature ratio. Globally, the changes which occur from now on, are similar in some aspects to those already noticed for the generalized Newtonian flows [1, 3].

In particular, for $\eta = 0.4$, for relatively small Weissenberg numbers ($We = 2, 3, 4$), and especially in the case of small curvature ratio, we observe a variation

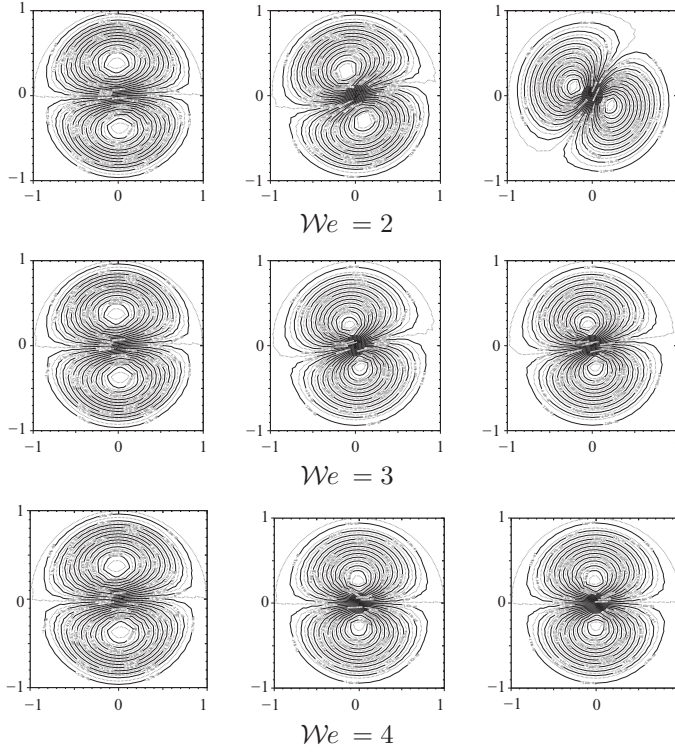


FIGURE 5. Streamlines for creeping generalized Oldroyd-B flows with $\eta=0.4$ and $|q| = 6, 6.4, 6.5$ (from left to right), for different Weissenberg numbers We ($\delta=0.001$).

in the shape of the vortices, their displacement to the core region, the concentration of the contours in this region and the beginning of a counter-clockwise rotation.

In Figure 5, we plot the streamlines corresponding to this case. The rotation is more pronounced when the Weissenberg number is small suggesting that the viscoelasticity, as well as the inertial forces in the case of generalized Newtonian flows, has an opposite effect [1, 3].

However, contrarily to the generalized Newtonian flows, the viscosity exponent corresponding to the initiation of the rotation is not constant. As can be seen in Table 2, it depends on We and as this parameter increases, the rotation initiates earlier. Moreover, the viscoelastic parameter affects the maximum angle and the development of the rotation: for $We = 2$, the contours are left-rotating (L), for $We = 3$ they are initially left-rotating and then right-rotating (R) before stabilizing symmetrically (S). Finally, when the We increases, there is no more rotation and the contours remain symmetric.

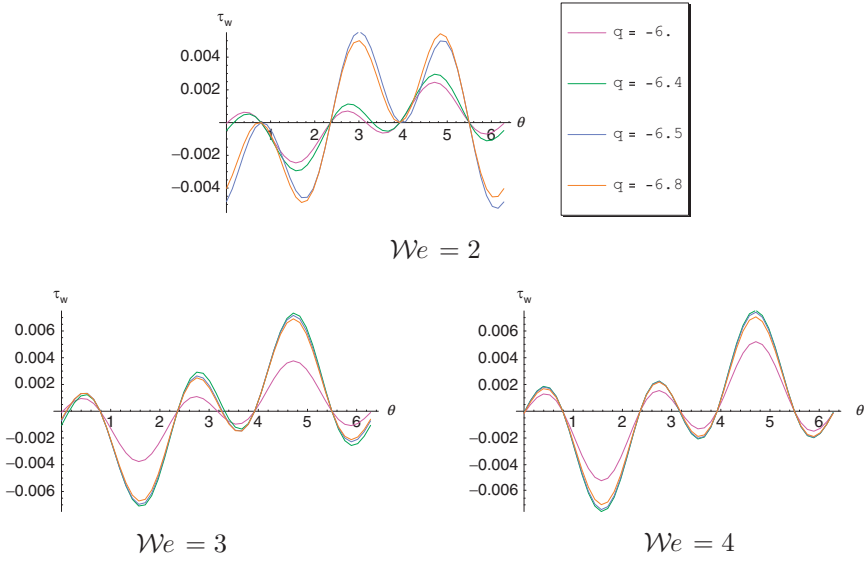


FIGURE 6. Wall shear stress for creeping generalized Oldroyd-B creeping flows with $\eta=0.4$ and $|q| = 6, 6.4, 6.5, 6.8$ ($\delta=0.001$).

We	2	3	4	5
$\delta = 0.001$				
$\eta = 0.4$	6.30 L	6.25 L-S	— S	— S
0.5	4.50 R	4.30 R(slight)	— S	— —

TABLE 2. Values of $|q|$ initiating the rotation.

Parallel modifications can be observed concerning the wall shear stress. Figure 6 shows the corresponding curves for $\eta = 0.4$ and for different values of the Weissenberg number. For $We = 5$, the curves corresponding to different viscosity exponents q are identical, suggesting that the wall shear stress is stable in this case. For $We = 4$, the global behavior of the curves is similar but with variations in the amplitudes. When the viscoelastic parameter is set to 3, small modifications could be observed in comparison to the previous case. In particular, for q greater than the critical value q_{var} initiating the rotation, we lose the symmetry with respect to the horizontal axis, and the wall shear stress takes negative values at $\theta = 0$ and 2π . This fact is more pronounced for $We = 2$, with loss of symmetry with respect to the axis $\theta = \pi$. The same differences are obtained when $\eta = 0.5$. The sign of the wall shear stress for values of q greater than q_{var} is positive. This strongly suggests

the existence of a relation between the sign of τ_w at the points $\theta = 0$ and 2π , and the orientation of the rotation.

A final observation is related to the maximum values of the stream function. Independently of the viscoelastic and viscosity parameters, the maximum values dramatically increase in the neighborhood of the critical value q_{var} . For the cases where the maximum value of the exponent q is big enough, we observe that after this peak, the maximum values decrease before stabilizing.

4.3.2. Inertial generalized Oldroyd-B flows. In the previous subsection, we studied the behavior of the generalized Oldroyd-B flows in the absence of inertia (creeping flows). Our aim here is to consider the more general case of inertial flows, and to analyse the effect of the Reynolds number in combination with the Weissenberg number, the viscosity parameter η , the exponent q , and the curvature ratio δ .

We first consider a pipe with a small curvature ratio ($\delta = 0.001$) in the case of a constant viscosity (inertial Oldroyd-B fluid). The secondary flows exist and the corresponding stream function and wall shear stress have globally the same behavior as the creeping Oldroyd-B flows. At this stage, the nature of the flow is qualitatively identical to that of a Newtonian fluid.

In order to compare with the case of generalized creeping flows, the viscosity parameter η is set to 0.4, 0.5, 0.6 and as previously, several tests were performed for different values of the Weissenberg and the Reynolds numbers, with a continuation in the exponent q .

One of the first remarks is that the *transition* phenomenon observed in the case of generalized creeping flows does not hold, even for relatively small Reynolds number ($Re = 15$). This fact is evident when η takes the values 0.4 and 0.5 and the behavior in these two cases is close to that of inertial generalized Newtonian flows.

Fixing $\eta = 0.4$, and varying the Reynolds and the Weissenberg numbers, the flow is globally stable for q less than some critical value. From the contours of the stream function and of the wall shear stress for the exponent $|q| \leq 5$, we observe that the qualitative behavior is similar and independent of both inertia and viscoelasticity. The only difference lies in the values and the magnitude of these quantities, which clearly depend on the involved parameters. In the neighborhood of a critical value of q , the behavior presents some changes and is no more uniform. The rotation already observed initiates, and its orientation depend on Re and We . Indeed, fixing the Reynolds number to 15, we can see that for $We = 2$, a counter-clockwise rotation occurs for $q_{\text{var}} = -6$ and that the contours remain stable till we reach the maximum value for which the convergence is ensured. For $We = 3$, the stream function initiates a very slight counter-clockwise rotation at the same value q_{var} , but recovers the symmetry very quickly. Finally, for $We = 3$, the same behavior is captured, but with a very slight clockwise rotation. The wall shear stresses behave in an analogous way. In order to emphasize the role of the inertia, we fixed the Weissenberg number and increase the Reynolds number.

In a second step, we consider the case $\eta = 0.5$. For $Re = 15$, we can observe that the Weissenberg number favors the clockwise rotation (cf. Figure 7). Indeed, when the Weissenberg number is small (even with larger exponent viscosity), the contours remain symmetric. As We increases, the rotation initiates and holds earlier. On the other hand, the Reynolds number does not seem to have a significative influence on the nature of the flow. We implement several tests corresponding to larger values of this characteristic parameter ($Re = 1, 15, 30, 50, 70$) and did not observe any significative difference.

Table 3 summarizes the results of the maximum values of viscosity parameter $|q|$ with respect to the viscoelasticity (We) and the inertia (Re) parameters, as a function of the curvature ratio (δ). For fixed δ and We , the value of $|q|$ decreases when Re increases. The same occurs if δ and Re are fixed: the value of $|q|$ decreases when We increases. The curvature ratio associated with (Re) and (We) has a strong influence on the convergence, since it can be shown that when these parameters increase, the values of $|q|$ decrease considerably and in some cases convergence is not achieved.

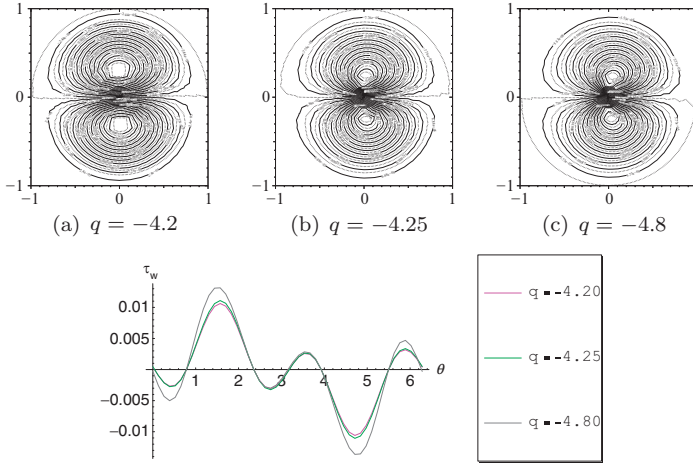


FIGURE 7. Streamlines and wall shear stress for inertial generalized Oldroyd-B flows with $\eta = 0.5$, $Re = 15$, $We = 1$ and different values of the $|q|$ ($\delta = 0.001$).

The case $\eta = 0.6$ is certainly the more surprising. For large values of the Reynolds number and for the achieved viscosity exponents, the behavior seems to be stable and no notable fact can be observed. The more interesting variations were observed for relatively small Reynolds numbers. Fixing for example $Re = 15$ and varying the Weissenberg number, we observe that the behavior is qualitatively stable for small values of this parameter. For $We = 3, 4$ and 5 , some new phenomenon initiates. The characteristics are very similar to those observed in the case

We	1	2	3	4	5
$\delta = 0.001$					
$Re = 1$	5.12	4.65	4.45	4.22	4.0
15	4.81	4.36	4.25	4.21	3.95
30	4.78	3.76	3.54	3.37	3.25
50	3.60	3.03	2.81	2.62	2.46
70	3.44	2.57	2.23	1.94	1.72
$\delta = 0.1$					
$Re = 1$	2.47	0.7	0.46	0.36	0.3
15	0.51	0.15	—	—	—
30	0.05	—	—	—	—
50	—	—	—	—	—
$\delta = 0.2$					
$Re = 1$	1.26	0.53	0.36	—	—
15	0.23	—	—	—	—
30	—	—	—	—	—

TABLE 3. Maximum values of $|q|$ with $\eta = 0.5$.

of generalized creeping flows during the *phase transition*: formation of boundary layers and a pair of new vortices or strengthening of the new contours and weakening of the original ones. However, in contrast with the creeping flows, the new state is not stable and at some level the inverse phenomenon initiates (Figure 8).

For this particular viscosity parameter, Table 4 shows the results of the maximum values of $|q|$, obtained for different We and Re numbers, in the case of $\delta = 0.001$. Comparing with Table 3 for the same curvature ratio, the same effects of viscoelasticity and inertia on $|q|$ can be observed.

We	1	2	3	4	5
$\delta = 0.001$					
$Re = 1$	3.10	2.89	2.68	2.6	2.56
15	2.88	2.67	2.60	2.55	2.51
70	1.69	1.39	1.20	1.05	0.95

TABLE 4. Maximum values of $|q|$ with $\eta = 0.6$.

5. Conclusion

This paper is devoted to finite element simulations of flows of incompressible viscoelastic non-Newtonian fluids of Oldroyd-type through pipes of uniform circular cross-section, and follows the work already published in [1] and [3] for generalized Newtonian fluids. We compare the quantitative and qualitative behavior of the

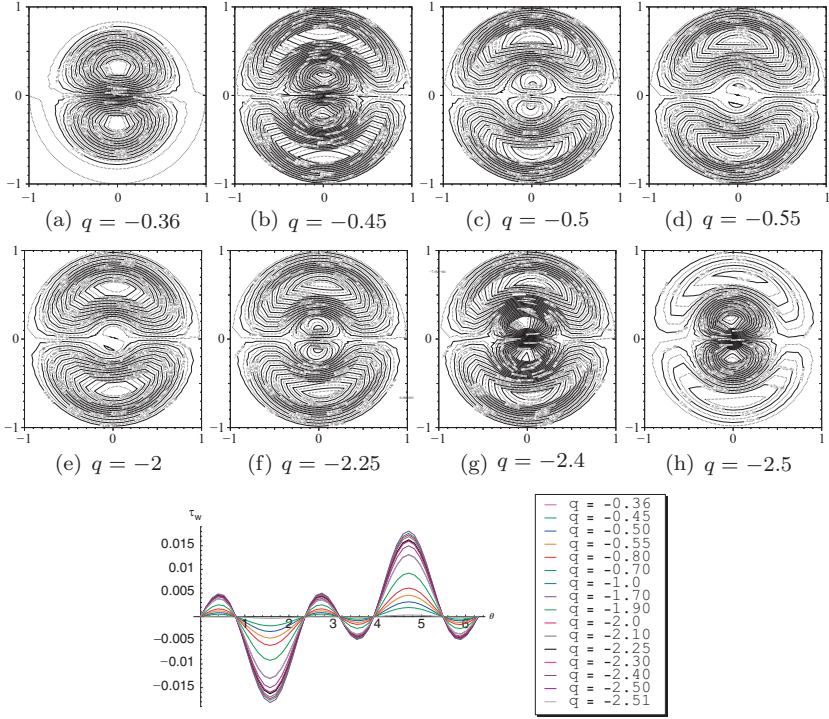


FIGURE 8. Streamlines and wall shear stress for inertial generalized Oldroyd-B flows with $\eta=0.6$, $Re=15$ and $We=5$ ($\delta=0.001$).

secondary streamlines and the wall shear stress for creeping and inertial generalized Oldroyd-B flows, performing computations for different values of the Reynolds number, the Weissenberg number, the curvature ratio and the non-dimensional viscosity parameters involved in the governing equations.

In particular, we observe interesting viscosity effects such that, for small curvature ratio and within a certain range of viscosity parameters, the secondary streamlines contours undergo a counter-clockwise rotation and lose symmetry. The complexity of the flow characteristics shown in the numerical tests suggest that further theoretical analysis is needed to study the existence of more than one solution and investigate the corresponding stability, for a range of appropriate non-dimensional parameters.

More detailed discussion and numerical results can be found in [19] where the generalized Newtonian flows are obtained as a particular case of generalized Oldroyd-B flows, in the limit of vanish Weissenberg number (neglected viscoelastic effects). The numerical validation of the present results, using the perturbation method [24] is a work in progress.

References

- [1] N. Arada, M. Pires and A. Sequeira, *Viscosity effects on flows of generalized Newtonian fluids through curved pipes*, Computers and Mathematics with Applications, **53** (2007), 625–646.
- [2] N. Arada, M. Pires and A. Sequeira, *Numerical approximation of viscoelastic Oldroyd-B flows in curved pipes*, RIMS, Kôkyûroku Bessatsu, **B1** (2007), 43–70.
- [3] N. Arada, M. Pires and A. Sequeira, *Numerical simulations of shear-thinning Oldroyd-B fluids in curved pipes*, IASME Transactions, **issue 6, Vol 2** (2005), 948–959.
- [4] A.A. Berger, L. Talbot and L.-S. Yao, *Flow in curved pipes*, Ann. Rev. Fluid Mech., **15** (1983), 461–512.
- [5] R.B. Bird, R.C. Armstrong and O. Hassager, *Dynamics of Polymeric Liquids*, John Wiley & Sons, New York (1987).
- [6] S. Chien, S. Usami, R.J. Dellembach, M.I. Gregersen, *Blood viscosity: influence of erythrocyte deformation*, Science **157** (3790), 827–829, 1967.
- [7] S. Chien, S. Usami, R.J. Dellembach, M.I. Gregersen, *Blood viscosity: influence of erythrocyte aggregation*, Science **157** (3790), 829–831, 1967.
- [8] P. Daskopoulos and A.M. Lenhoff, *Flow in curved ducts: bifurcation structure for stationary ducts*, J. Fluid Mech., **203** (1989), 125–148.
- [9] W.R. Dean, *Note on the motion of fluid in curved pipe*, Philos. Mag., **20**, **208** (1927).
- [10] W.R. Dean, *The streamline motion of fluid in curved pipe*, Philos. Mag., **30**, **673** (1928).
- [11] J. Eustice, *Flow of water in curved pipes*, Proc. R. Soc. Lond. A **84** (1910), 107–118.
- [12] J. Eustice, *Experiments of streamline motion in curved pipes*, Proc. R. Soc. Lond. A **85** (1911), 119–131.
- [13] Y. Fan, R.I. Tanner and N. Phan-Thien, *Fully developed viscous and viscoelastic flows in curved pipes*, J. Fluid Mech., **440** (2001), 327–357.
- [14] J.H. Grindley and A.H. Gibson, *On the frictional resistance to the flow of air through a pipe*, Proc. R. Soc. Lond. A **80** (1908), 114–139.
- [15] D.D. Joseph, *Fluid Dynamics of Viscoelastic Liquids*, Springer Verlag, New York (1990).
- [16] R. Keunings, *A Survey of Computational Rheology*, In: Proceedings of the XIII International Congress on Rheology (D.M. Binding et al. ed.), *British Soc. Rheol.*, **1** (2000), 7–14.
- [17] R. Owens and T.N. Phillips, *Computational Rheology*, Imperial College Press, London (2002).
- [18] T.J. Pedley, *Fluid Mechanics of Large Blood Vessels*, Cambridge University Press, Cambridge (1980).
- [19] M. Pires, *Mathematical and Numerical Analysis of Non-Newtonian Fluids in Curved Pipes*, PhD thesis, IST, Lisbon (2005)
- [20] K.R. Rajagopal, *Mechanics of non-Newtonian Fluids*, Galdi, G.P. and J. Nečas (eds.) *Recent Developments in Theoretical Fluid Mechanics*, Pitman Research Notes in Mathematics 291 (1993), Longman Scientific and Technical, 129–162.
- [21] M. Renardy, *Mathematical Analysis of Viscoelastic Flows*, SIAM (2000).

- [22] M. Renardy, W.J. Hrusa and J.A. Nohel, *Mathematical problems in Viscoelasticity*, Pitman Monographs and Surveys in Pure and Applied Mathematics, Longman **35** (1987).
- [23] A.M. Robertson, *On viscous flow in curved pipes of non-uniform cross section*, Inter. J. Numer. Meth. fluid., **22** (1996), 771–798.
- [24] A.M. Robertson and S.J. Muller, *Flow of Oldroyd-B fluids in curved pipes of circular and annular cross-section*, Int. J. Non-Linear Mechanics, **31** (1996), 1–20.
- [25] A.M. Robertson, A. Sequeira and M. Kameneva, *Hemorheology*, Hemodynamical Flows: Modeling, Analysis and Simulation, Series: Oberwolfach Seminars, G.P. Galdi, R. Rannacher, A.M. Robertson, S. Turek, Birkhäuser, **37** (2008), 63–120.
- [26] W.R. Schowalter, *Mechanics of Non-Newtonian Fluids*, Pergamon Press, New York (1978).
- [27] W.Y. Soh and S.A. Berger, *Fully developed flow in a curved pipe of arbitrary curvature ratio*, Int. J. Numer. Meth. Fluid., **7** (1987), 733–755.
- [28] G.B. Thurston, *Viscoelasticity of human blood*, Biophys. J., **12** (1972), 1205–1217.
- [29] C. Truesdell and W. Noll, *The Non-Linear Field Theories of Mechanics*, Encyclopedia of Physics, (ed. S. Flugge), **vol.III/3** (1965), Springer-Verlag.
- [30] G.S. Williams, C.W. Hubbell and G.H. Fenkell, *Experiments at Detroit, Mich. on the effect of curvature upon the flow of water in pipes*, Trans. ASCE **47** (1902), 1–196.
- [31] Z.H. Yang and H.B. Keller, *Multiple laminar flows through curved pipes*, Appl. Numer. Math., **2** (1986), 257–271.

Marília Pires

Centro de Investigação em Matemática e Aplicações

Universidade de Évora

Rua Romão Ramalho,

7000-671 Évora

Portugal

e-mail: marilia@uevora.pt

Adélia Sequeira

Centro de Matemática e Aplicações

Instituto Superior Técnico

Av. Rovisco Pais,

1049-001 Lisboa

Portugal

e-mail: adelia.sequeira@math.ist.utl.pt

Parabolic Problems

The Herbert Amann Festschrift

Escher, J.; Guidotti, P.; Hieber, M.; Mucha, P.; Prüss,
J.W.; Shibata, Y.; Simonett, G.; Walker, C.; Zajackowski,
W. (Eds.)

2011, XII, 717 p. 15 illus., 7 illus. in color., Hardcover

ISBN: 978-3-0348-0074-7

A product of Birkhäuser Basel